



Bacterial alginate regulators and phage homologs repress CRISPR–Cas immunity

Adair L. Borges¹, Bardo Castro¹, Sutharsan Govindarajan^{1,4}, Tina Solvik¹, Veronica Escalante¹ and Joseph Bondy-Denomy^{1,2,3}✉

CRISPR–Cas systems are adaptive immune systems that protect bacteria from bacteriophage (phage) infection¹. To provide immunity, RNA-guided protein surveillance complexes recognize foreign nucleic acids, triggering their destruction by Cas nucleases². While the essential requirements for immune activity are well understood, the physiological cues that regulate CRISPR–Cas expression are not. Here, a forward genetic screen identifies a two-component system (KinB–AlgB), previously characterized in the regulation of *Pseudomonas aeruginosa* alginate biosynthesis^{3,4}, as a regulator of the expression and activity of the *P. aeruginosa* Type I–F CRISPR–Cas system. Downstream of KinB–AlgB, activators of alginate production AlgU (a σ^E orthologue) and AlgR repress CRISPR–Cas activity during planktonic and surface-associated growth⁵. AmrZ, another alginate regulator⁶, is triggered to repress CRISPR–Cas immunity upon surface association. *Pseudomonas* phages and plasmids have taken advantage of this regulatory scheme and carry hijacked homologs of AmrZ that repress CRISPR–Cas expression and activity. This suggests that while CRISPR–Cas regulation may be important to limit self-toxicity, endogenous repressive pathways represent a vulnerability for parasite manipulation.

Type I CRISPR–Cas systems are comprised of a multisubunit RNA-guided surveillance complex, a *trans*-acting nuclease (Cas3)^{7,8} and proteins dedicated to spacer acquisition, Cas1 and Cas2⁹. *P. aeruginosa* has become a powerful model organism for studying Type I CRISPR–Cas mechanisms^{10–15}, functions^{16–19}, evolution^{20–22} and interactions with phages using anti-CRISPR proteins^{23–26}. The *P. aeruginosa* strain PA14 possesses a naturally active Type I–F CRISPR–Cas immune system, comprising two CRISPR arrays, an operon encoding surveillance complex subunits Csy1–4¹² and a separate operon encoding Cas1 and a Cas2–3 fusion protein. Quorum sensing has been shown to activate CRISPR–Cas expression in *P. aeruginosa*²⁷ and other species of bacteria²⁸. However, little is known about the factors that temper CRISPR–Cas activity and mitigate the risk of acquiring and expressing a nucleolytic immune system.

To discover new CRISPR–Cas regulators in *P. aeruginosa*, we used *P. aeruginosa* strain PA14 engineered to express *lacZ* in place of the *csy3* gene (*csy3::lacZ*)¹⁷. This strain was subjected to C9 *mariner* transposon mutagenesis and ~40,000 colonies were screened on X-gal plates. Multiple independent insertions were identified within *lacZ* and upstream genes (*csy1* and *csy2*) and 30 mutants with transposon insertions outside of this region were isolated and mapped (Extended Data Fig. 1). Four independent insertions were identified in a single gene, *kinB*, which resulted in decreased β -galactosidase

production on solid plates (Extended Data Fig. 2a) and ~30% less *csy3::lacZ* activity in liquid culture compared with the unmutagenized parent (Extended Data Fig. 2b). We selected *kinB* (a sensor kinase/phosphatase) for follow-up study as it had the most independent transposon insertions and displayed the largest β -galactosidase activity change.

We measured the ability of *kinB::Tn* insertions to limit the survival and replication of phages when introduced into the wild-type (WT; CRISPR-active) strain. The phages used to assay activity were: DMS3_{*acrIE3*}, which is an untargeted control phage, DMS3m_{*acrIE3*}¹⁸, which is fully targeted by the PA14 Type I–F CRISPR–Cas system, and phage DMS3m_{*acrIF4*}, which is partially targeted, by virtue of encoding a ‘weak’ anti-CRISPR, *acrIF4*, that binds to the surveillance complex to inhibit CRISPR–Cas function^{23,25,29}. The *kinB::Tn* strains remained resistant to DMS3m_{*acrIE3*} infection, but we observed a tenfold increase in DMS3m_{*acrIF4*} plaque-forming units (p.f.u.) relative to WT, demonstrating attenuated CRISPR–Cas activity (Fig. 1a, Extended Data Fig. 2c). This defect was complemented by the expression of *kinB* in *trans* (Extended Data Fig. 2c). The growth of control phage DMS3_{*acrIE3*} was not impacted in the absence of *kinB* (Fig. 1a, Extended Data Fig. 2c). Furthermore, two other phages that are partially targeted, JBD26 (which naturally possesses *acrIF4*) and JBD25 (a phage with no Acr that is targeted by a weak spacer that provides incomplete immunity), also showed increased survival in the *kinB::Tn* strain (Extended Data Fig. 2d) relative to WT PA14. The survival of a phage with a weak anti-CRISPR or one that is targeted by a less active spacer is therefore a sensitive barometer for perturbations in CRISPR–Cas levels. Together, these data confirm that in the absence of *kinB*, *csy* gene expression and phage targeting are decreased.

KinB is a sensor kinase/phosphatase in a two-component system with response regulator AlgB. The KinB–AlgB system has a large regulon within *P. aeruginosa* and controls the biosynthesis of the extracellular polysaccharide alginate⁴. This pathway is well studied due to the recurrent isolation of alginate-overproducing (mucoid) *P. aeruginosa* from the lungs of cystic fibrosis patients, where alginate plays an important role in the formation of antibiotic-resistant biofilms during chronic infection. The absence of KinB function results in the accumulation of the phosphorylated form of the response regulator AlgB (P-AlgB), while the phosphorylation of AlgB has been attributed to unknown kinases^{30,31} (Fig. 1b). P-AlgB activates the periplasmic protease AlgW (a DegS homolog), which degrades MucA, liberating sigma factor AlgU^{3,32,33} (Fig. 1b). AlgU positively regulates many factors involved in alginate production, including AlgR, AlgD, AlgB and AmrZ^{5,6,34}.

¹Department of Microbiology & Immunology, University of California, San Francisco, San Francisco, CA, USA. ²Quantitative Biosciences Institute, University of California, San Francisco, San Francisco, CA, USA. ³Innovative Genomics Institute, Berkeley, CA, USA. ⁴Present address: Department of Biology, SRM University AP, Amaravati, India. ✉e-mail: joseph.bondy-denomy@ucsf.edu

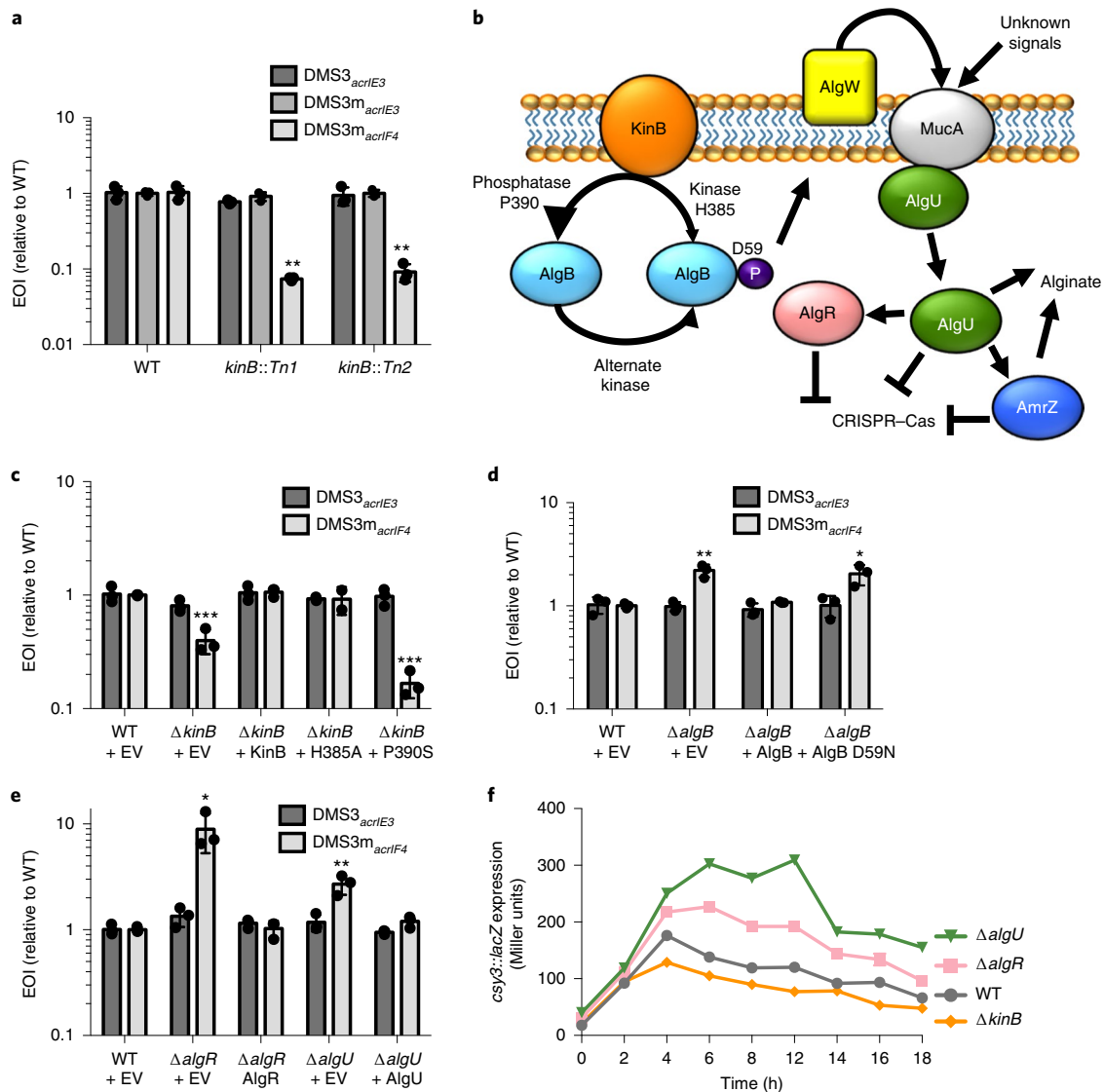


Fig. 1 | A forward genetic screen identified a role for an alginate-activating pathway in the repression of CRISPR-Cas immunity. **a**, The EOI against isogenic phages DMS3_{acrIE3} (non-targeted), DMS3m_{acrIE3} (no I-F anti-CRISPR, CRISPR-targeted) and DMS3m_{acrIF4} (weak I-F anti-CRISPR, CRISPR-targeted). The p.f.u. quantified on two independent *kinB* transposon mutants (*kinB::Tn1* and *kinB::Tn2*) are presented as a ratio relative to the number of p.f.u. measured on WT PA14. Tn mutants show an altered EOI against DMS3m_{acrIF4} relative to WT (*Tn1*: $P = 2.9 \times 10^{-3}$; *Tn2*: $P = 3.2 \times 10^{-3}$). **b**, A cartoon summarizing the KinB-AlgB two-component system and downstream effects, based on previous work⁴⁹ (see text) with CRISPR-Cas regulation added. **c-e**, EOI measurements for indicated $\Delta kinB$ (**c**), $\Delta algB$ (**d**), and $\Delta algR$ and $\Delta algU$ strains (**e**) with complementation. Mutants show an altered EOI against DMS3m_{acrIF4} relative to WT ($\Delta kinB$ + empty vector (EV): $P = 4.30 \times 10^{-4}$; $\Delta kinB$ + P390S: $P = 5.6 \times 10^{-6}$; $\Delta algB$ + EV: $P = 2.8 \times 10^{-3}$; $\Delta algB$ + D59N: $P = 1.8 \times 10^{-2}$; $\Delta algR$ + EV: $P = 1.9 \times 10^{-2}$; $\Delta algU$ + EV: $P = 6.6 \times 10^{-3}$). **f**, *csy3::lacZ* β -galactosidase activity over time in the indicated strain backgrounds. The experiment was replicated twice with fewer time points and consistent results were seen. All EOI data are presented as the mean of three biological replicates \pm s.d. β -galactosidase reporter activity is presented as the mean of three technical replicates. A two-tailed unpaired Student's *t*-test was used to calculate *P* values; * $P < 0.05$, ** $P < 0.01$, *** $P < 0.001$.

WT *kinB* or kinase-inactive H385A *kinB* complemented an in-frame $\Delta kinB$ deletion, restoring CRISPR targeting of DMS3m_{acrIF4} (Fig. 1c). However, a P390S *kinB* mutant incapable of dephosphorylating the response regulator AlgB did not complement CRISPR-Cas activity and in fact decreased it further (Fig. 1c). A $\Delta kinB \Delta algB$ double mutant restored CRISPR-Cas targeting to levels twofold above the WT (Extended Data Fig. 3b), confirming the role of this signalling pathway. A strain lacking *algB* ($\Delta algB$) or possessing a D59N mutant that cannot be phosphorylated also elevated CRISPR-Cas activity twofold, supporting the repressive role of P-AlgB (Fig. 1d). These data show that the accumulation of high levels of

P-AlgB (achieved in *kinB::Tn*, $\Delta kinB$ or *kinB* P390S) led to CRISPR-Cas repression.

We next assayed antiphage immunity in $\Delta algU$ and $\Delta algR$ backgrounds, revealing increased targeting of DMS3m_{acrIF4} but not control phage DMS3_{acrIE3} in both knockouts (Fig. 1e). Complementation restored CRISPR-Cas levels (Fig. 1e), demonstrating that AlgU and AlgR repress CRISPR-Cas immunity. Double knockouts of each gene combined with $\Delta kinB$ also demonstrated increased CRISPR-Cas immunity, consistent with these factors acting as repressors downstream of KinB (Extended Data Fig. 3a). All changes in DMS3m_{acrIF4} phage replication and survival were CRISPR dependent, as double

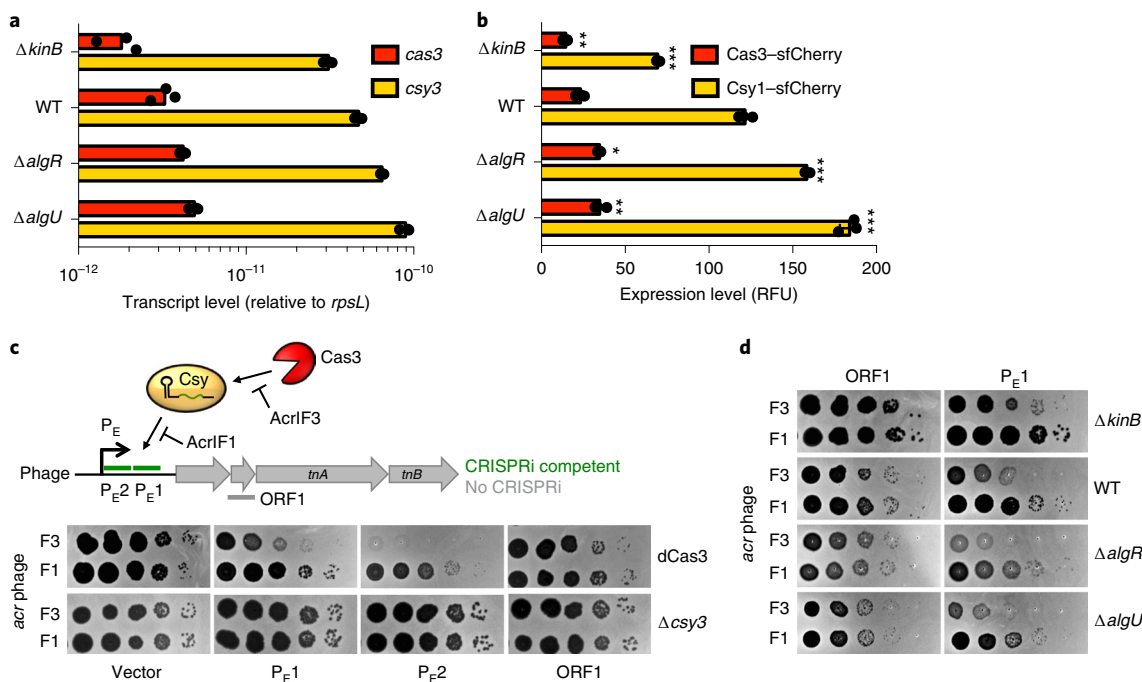


Fig. 2 | The KinB–AlgB pathway modulates Cas3 and Csy protein and RNA levels. **a**, RT–qPCR measurements of the transcript levels of *cas3* and *csy3* normalized to the housekeeping gene *rpsL* after 8 h of growth in liquid culture. The measurements are presented as the mean of three technical replicates. **b**, The measurement of the fluorescence levels (in relative fluorescence units (RFU)) of Cas3–sfCherry or Csy1–sfCherry reporter strains after 10 h of growth in liquid culture. Fluorescence measurements are presented as the mean of three biological replicates \pm s.d. Mutants show altered Cas3–sfCherry levels ($\Delta kinB$: $P = 7.8 \times 10^{-3}$; $\Delta algR$: $P = 1.5 \times 10^{-4}$; $\Delta algU$: $P = 1.1 \times 10^{-4}$) and Csy1–sfCherry levels relative to WT ($\Delta kinB$: $P = 3.3 \times 10^{-5}$; $\Delta algR$: $P = 1.5 \times 10^{-4}$; $\Delta algU$: $P = 1.1 \times 10^{-4}$). A two-tailed unpaired Student's *t*-test was used to calculate *P* values; * $P < 0.05$, ** $P < 0.01$, *** $P < 0.001$. **c**, A spot titration of F3 (DMS3m_{acrIF3}) or F1 (DMS3m_{acrIF1}) on dCas3 or active Cas3 ($\Delta csy3$; no Csy complex) strains. Phages were targeted by the natural spacer CR2_sp1 and crRNAs designed to target the DMS3m genome in the positions designated on the ORF map. Green lines indicate crRNA binding positions mediating CRISPRi; the grey line indicates positions that do not mediate CRISPRi. **d**, A spot titration of DMS3m_{acrIF3} and DMS3m_{acrIF1} phages on WT PA14 or deletion mutants expressing the indicated crRNA. Plaquing experiments were replicated three times and consistent results were seen.

knockouts (*kinB*, *algB*, *algU* and *algR* mutants combined with *csy3::lacZ*, a loss-of-function mutation) revealed plaquing equivalent to *csy3::lacZ* alone (Extended Data Fig. 3b). β -galactosidase activity was measured in these strains during growth in liquid culture, revealing a peak in *csy* expression around 8 h, with repression of this operon during entry into the stationary phase (Fig. 1f). As suggested by the phage-targeting experiments, a marked increase in the expression of the *csy* operon was noted for both $\Delta algR$ and $\Delta algU$ strains, with a decrease in *csy* expression for $\Delta kinB$.

Next, we performed quantitative PCR with reverse transcription (RT–qPCR) of the *cas3* and *csy3* transcripts in the mutant strains. We measured the relative abundance of Cas3 and Csy complex proteins by fusing a sfCherry tag to the endogenous *cas3* or *csy1* gene in the mutant backgrounds, using fluorescence as a proxy for protein abundance. We found that *kinB* loss decreased the expression of both the *cas3* and *csy* operons, resulting in lower *cas3* and *csy3* transcript levels and Cas3–sfCherry and Csy1–sfCherry levels relative to WT (Fig. 2a,b). Conversely, we observed increased levels of *cas3* and *csy3* transcripts and Cas3–sfCherry and Csy1–sfCherry in the $\Delta algR$ and $\Delta algU$ mutants relative to WT (Fig. 2a,b). These data demonstrate that this pathway controls the levels of both Cas3 and the Csy complex in the bacterial cell by transcriptionally controlling the *cas3* and *csy* operons.

As Cas3–sfCherry was expressed at low levels relative to Csy1–sfCherry, and is also known to be subject to post-translational control by Cas1¹⁴, we sought to dissect the relative contributions of nuclease versus surveillance complex dysregulation to the immune phenotypes of the KinB–AlgB pathway mutants. To specifically measure the antiphage activity of the Csy complex, we developed a

Cas3-independent bioassay to read out the activity of the surveillance complex in the cell. Through the rational design of CRISPR RNAs (crRNAs) to target an early phage promoter (P_{E1} , P_{E2}), we observed the inhibition of phage survival in a *P. aeruginosa* strain with a nuclease dead Cas3 (dCas3), while an open reading frame (ORF)-targeting crRNA (ORF1) was ineffective (Fig. 2c). Remarkably, this CRISPR-based transcriptional interference (CRISPRi) effect was strong enough to completely limit phage replication in the absence of Cas3 nuclease activity for crRNA P_{E2} . Phage inhibition via CRISPRi occurred during infection with a phage that expressed the inhibitor of Cas3 recruitment, AcrIF3, but not an inhibitor that blocked Csy complex–phage DNA binding²⁵, AcrIF1 (Fig. 2c). We selected P_{E1} as a moderately functional CRISPRi spacer and expressed it in KinB–AlgB pathway mutants. We observed decreased CRISPRi activity against phage DMS3m_{acrIF3} in the $\Delta kinB$ background, but increased CRISPRi in $\Delta algR$ and $\Delta algU$ (Fig. 2d; compare F3 and F1 phage). This demonstrates that the modulation of *csy* gene expression is sufficient to impact phage targeting in a Cas3-independent manner. We conclude that the KinB–AlgB pathway regulates Cas3 and Csy complex levels and that the repression of Csy complex levels has a large impact on antiphage immunity.

To identify downstream CRISPR–Cas regulators in the AlgU regulon³⁵, we focused on another factor involved in alginate production, alginate and motility regulator Z, *amrZ*³⁶. We generated a knockout of *amrZ* and observed a CRISPR-dependent increase in efficiency of immunity (EOI) against phage DMS3m_{acrIF4} (Fig. 3a, Extended Data Fig. 3b). This was complemented when *amrZ* was expressed in *trans* (Fig. 3a). A $\Delta kinB\Delta amrZ$ double knockout also showed increased CRISPR–Cas activity, consistent with its

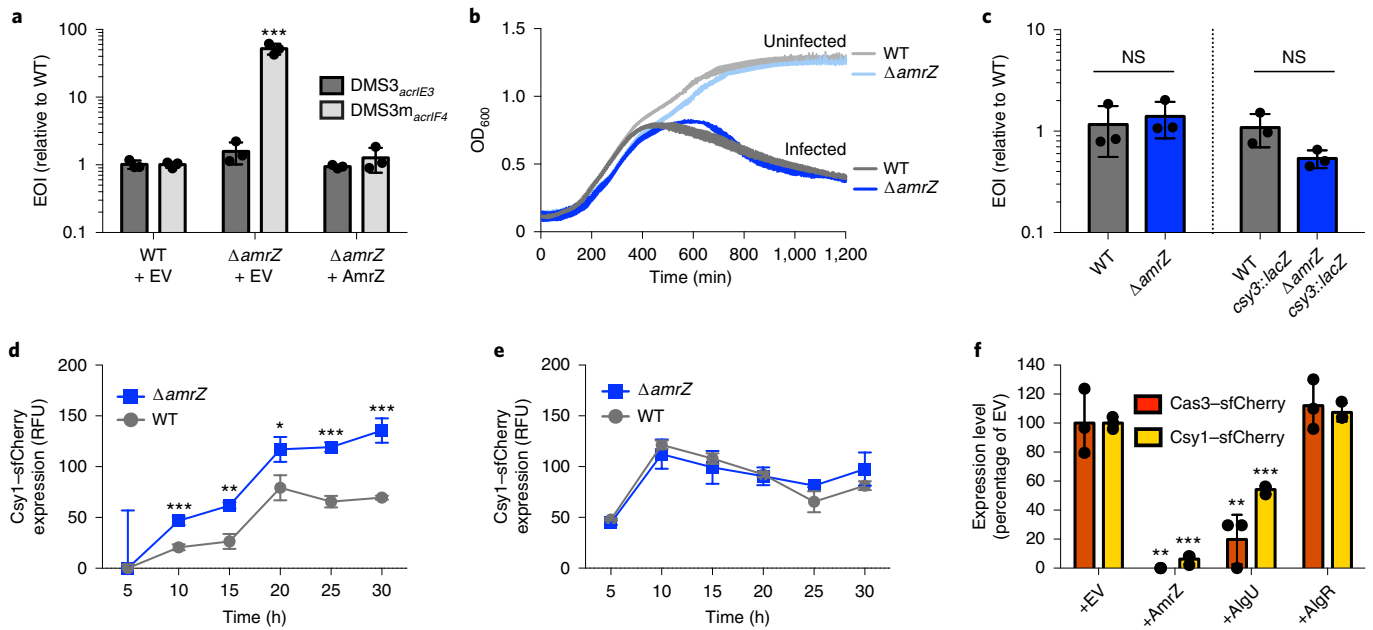


Fig. 3 | AmrZ is a surface-activated repressor of CRISPR-Cas immunity. **a**, The EOI against phages DMS3_{acrIE3} (non-targeted) and DMS3m_{acrIF4} (CRISPR-targeted) during surface association. The p.f.u. values were quantified on $\Delta amrZ$ or the complemented strain and are presented as a ratio of the number of p.f.u. measured on WT PA14. $\Delta amrZ$ + EV shows increased EOI against DMS3m_{acrIF4} relative to WT ($P=7.3 \times 10^{-4}$). EOI measurements are presented as the mean of three biological replicates \pm s.d. **b**, Growth curves of liquid cultures of PA14 WT and $\Delta amrZ$ infected with 10^6 p.f.u. of virulent DMS3m_{acrIF4} alongside uninfected controls. **c**, EOI against virulent DMS3m_{acrIF4} in liquid cultures of WT and $\Delta amrZ$ strains (CRISPR active) or WT *csy3::lacZ* and $\Delta amrZ$ *csy3::lacZ* (CRISPR inactive). The p.f.u. were quantified after 24 h from $\Delta amrZ$ or *amrZ* *csy3::lacZ*, then presented as a ratio of p.f.u. from WT or WT *csy3::lacZ*, respectively. Bacterial optical density measured at 600 nm (OD_{600}) and EOI measurements are presented as the mean of three biological replicates \pm s.d. $\Delta amrZ$ and $\Delta amrZ$ *csy3::lacZ* show no significant difference in EOI relative to WT and WT *csy3::lacZ*, respectively ($\Delta amrZ$: $P=0.6$; $\Delta amrZ$ *csy3::lacZ*: $P=0.08$). **d, e**, The time course of the fluorescence levels (RFU) of Csy1-sfCherry reporter strains during surface association (relative to WT (10 h: $P=8.9 \times 10^{-4}$; 15 h: $P=1.5 \times 10^{-3}$; 20 h: $P=2.0 \times 10^{-2}$; 25 h: $P=2.2 \times 10^{-4}$; 30 h: $P=7.0 \times 10^{-4}$)) or planktonic growth (e). $\Delta amrZ$ has increased Csy1-sfCherry levels during surface association relative to WT (10 h: $P=8.9 \times 10^{-4}$; 15 h: $P=1.5 \times 10^{-3}$; 20 h: $P=2.0 \times 10^{-2}$; 25 h: $P=2.2 \times 10^{-4}$; 30 h: $P=7.0 \times 10^{-4}$). **f**, Normalized fluorescence measurements of WT Cas3-sfCherry or Csy1-sfCherry overexpressing the indicated transcription factors after 10 h growth in liquid culture. AmrZ and AlgU overexpression reduced Cas3-sfCherry (AmrZ: $P=1.5 \times 10^{-3}$; AlgU: $P=7.8 \times 10^{-3}$) and Csy1-sfCherry (AmrZ: $P=7.5 \times 10^{-6}$; AlgU: $P=9.9 \times 10^{-5}$) levels relative to WT. Fluorescence measurements are presented as the mean of three biological replicates \pm s.d. A two-tailed unpaired Student's *t*-test was used to calculate *P* values; NS, not significant; * $P < 0.05$, ** $P < 0.01$, *** $P < 0.001$.

role as a repressor downstream of KinB (Extended Data Fig. 3a). However, when we measured *cas3* and *csy3* transcript levels and Cas3-sfCherry and Csy1-sfCherry levels in $\Delta amrZ$, neither transcript nor protein levels differed from the WT (Extended Data Fig. 4a,b). In considering these discrepant results, we realized that the antiphage plaque assay was performed on solid plates whereas RNA quantification and sfCherry fluorescence measurements were conducted on liquid culture samples. To measure the antiphage activity of $\Delta amrZ$ in planktonic growth, we challenged WT and $\Delta amrZ$ with 10^6 plaque-forming units (p.f.u.; multiplicity of infection=0.2) of virulent DMS3m_{acrIF4} in liquid culture. Both strains succumbed to phage infection with similar kinetics (Fig. 3b) and phage replication did not differ significantly between the two strains (Fig. 3c). Phage replication in the absence of CRISPR-Cas immunity also did not differ between the two strains (Fig. 3c). This demonstrates that, under our conditions, AmrZ does not control CRISPR-Cas during planktonic growth.

To test the hypothesis that AmrZ is a surface-activated repressor of CRISPR-Cas, we measured the levels of Csy complex during surface association and planktonic growth in WT and $\Delta amrZ$ cells using an endogenous Csy1-sfCherry reporter over a period of 30 h. In WT cells, the levels of Csy complex were attenuated during surface association relative to planktonic growth (~50% reduction of peak Csy1-sfCherry levels; Fig. 3d), but in the absence of AmrZ, Csy complex levels during surface association increased to levels comparable to those in planktonic growth (Fig. 3d). The deletion

of *amrZ* did not impact Csy complex levels in liquid culture at any time point (Fig. 3e). To increase the levels of AmrZ during planktonic growth, we ectopically expressed AmrZ from a high-copy plasmid and measured the impact on our transcriptional reporter *csy3::lacZ* and our translational reporters Csy1-sfCherry and Cas3-sfCherry. Here, high levels of AmrZ in liquid growth reduced the β -galactosidase activity of the *csy3::lacZ* reporter (Extended Data Fig. 4c) and greatly limited the expression of Csy1-sfCherry and Cas3-sfCherry (Fig. 3f). These results suggest that low AmrZ activity in planktonic growth underlies its surface-activated control of CRISPR-Cas. In contrast to AmrZ, overexpression of AlgU only moderately impacted Csy complex and Cas3 levels and AlgR did not impact the levels of either reporter when overexpressed (Fig. 3f).

We next considered whether phages and other mobile genetic elements (MGEs) had evolved mechanisms to manipulate this CRISPR-Cas repressive pathway. Inspired by the discovery of a *Paraburkholderia* phage that carried a distant homolog of AmrZ³⁷, we searched the National Center for Biotechnology Information (<https://www.ncbi.nlm.nih.gov/>) database for AmrZ homologs on *Pseudomonas* MGEs. We identified 15 diverse *Pseudomonas* mobile elements carrying AmrZ homologs (Extended Data Fig. 5). These MGEs included obligately lytic and temperate Myophages, temperate Siphophages and plasmids. AmrZ has been structurally characterized in complex with operator DNA³⁸ and these mobile AmrZ homologs showed perfect conservation of critical DNA-interacting residues in the ribbon-helix-helix domain, suggesting conserved

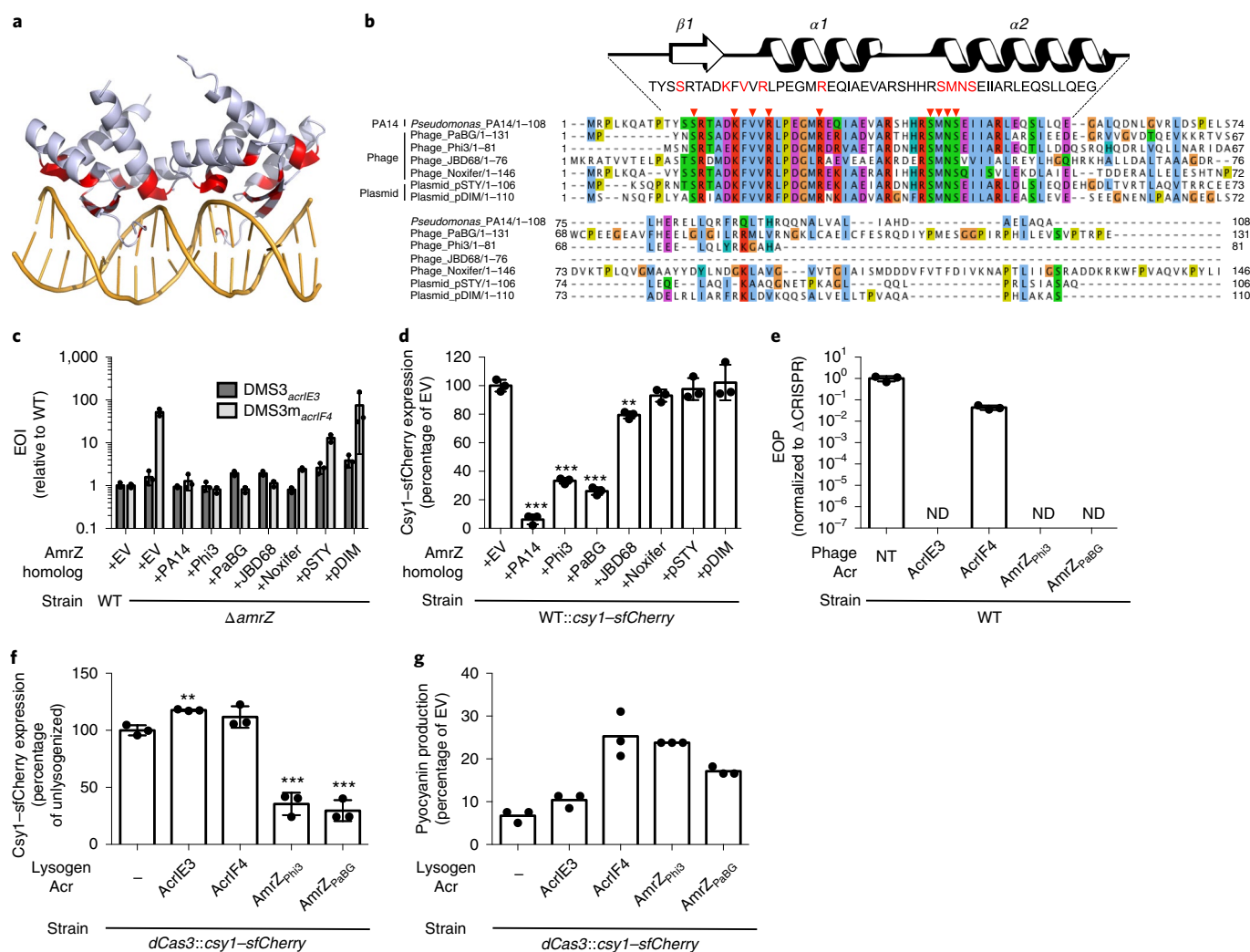


Fig. 4 | Phage-derived AmrZ homologs control CRISPR–Cas immunity. **a**, The structure of an AmrZ tetramer bound to 18 base pairs (bp) of operator DNA³⁸ with DNA-contacting residues highlighted in red. **b**, The alignment of six mobile AmrZ homologs and the native PA14 AmrZ homolog, with the ribbon-helix-helix DNA-binding domain schematized and DNA-contacting residues indicated with red arrows and text. Amino acids are coloured by chemical profile and numbered by position. **c**, The EOI against DMS3_{acrIE3} (non-targeted) and DMS3m_{acrIF4} (CRISPR-targeted). The p.f.u. were quantified on $\Delta amrZ$ or the strains complemented with AmrZ homologs, then presented as a ratio to the number of p.f.u. measured on WT PA14. The measurements are presented as the mean of three biological replicates \pm s.d. **d**, Normalized fluorescence levels of Csy1–sfCherry reporter strains expressing AmrZ homologs after 10 h of growth in liquid culture, shown as the mean of three biological replicates \pm s.d. AmrZ homologs from PA14, Phi3, PaBG and JBD68 repressed Csy1–sfCherry relative to the WT (PA14: $P=7.5 \times 10^{-6}$; Phi3: $P=1.5 \times 10^{-5}$; PaBG: $P=1.3 \times 10^{-5}$; JBD68: $P=1.9 \times 10^{-3}$). **e**, The efficiency of plaquing (EOP) of non-targeted DMS3_{acrIE3} phage (NT) or targeted DMS3m_{acr} phages. The EOP is the ratio of p.f.u. on PA14 WT to p.f.u. measured on PA14 Δ CRISPR, presented as the mean of three biological replicates \pm s.d. ND, not detectable. **f**, Fluorescence levels of *dCas3::csy1-sfCherry* after 16 h of liquid growth lysogenized with the indicated DMS3m_{acr} phage, normalized to the unlysogenized control (–) and presented as the mean of three biological replicates \pm s.d. The expression of AmrZ_{Phi3} ($P=4.9 \times 10^{-4}$) and AmrZ_{PaBG} ($P=2.8 \times 10^{-4}$) from a prophage repressed Csy1–sfCherry expression relative to an unlysogenized control. **g**, Pyocyanin production from *dCas3::csy1-sfCherry* reporter strains lysogenized with the indicated DMS3m_{acr} phage or the unlysogenized control (–) after 16 h of growth in liquid culture. Pyocyanin levels during *phzM* targeting are shown as a percentage of pyocyanin levels in an EV control and presented as the mean of three technical replicates. The experiment was replicated three times and consistent results were seen. A two-tailed unpaired Student's *t*-test was used to calculate *P* values; ** $P < 0.01$, *** $P < 0.001$.

binding specificity (Fig. 4a,b, red residues/arrowheads). To test whether these mobilized AmrZ variants were capable of regulating CRISPR–Cas activity in *P. aeruginosa*, we assayed the ability of six MGE-encoded AmrZ homologs to complement the $\Delta amrZ$ strain. Five out of six MGE-encoded homologs complemented the $\Delta amrZ$ mutant to various degrees, indicating that they were active in the PA14 transcriptional network and were bona fide CRISPR–Cas regulators (Fig. 4c). Next, each gene was expressed in WT cells, which revealed that three *P. aeruginosa* phage AmrZ homologs (AmrZ_{PaBG}, AmrZ_{Phi3}, AmrZ_{JBD68}) inhibited Csy complex biogenesis (Fig. 4d).

We next studied the anti-CRISPR function of these mobilized AmrZ homologs in the context of the phage life cycle. By inserting the two most potent phage AmrZ homologs, *amrZ*_{Phi3} and *amrZ*_{PaBG}, into the anti-CRISPR locus of phage DMS3m, we compared the anti-CRISPR capacity of these repressors relative to bona fide Type I-F inhibitor AcrIF4 and the negative control inhibitor AcrIE3. The AmrZ homologs provided no protection during lytic growth (Fig. 4e), likely because they cannot act on previously synthesized CRISPR–Cas complexes. However, they were able to significantly reduce the expression and activity of the CRISPR–Cas complex

during lysogeny (Fig. 4f,g). By lysogenizing a strain of PA14 with a catalytically dead Cas3 and an endogenously tagged copy of Csy1-sfCherry, we demonstrated that the presence of AmrZ_{Phi3} or AmrZ_{PaBG} reduced Csy complex levels to less than 50% of an unlysogenized control, while AcrIE3 and AcrIF4 did not reduce Csy complex levels (Fig. 4f). To measure the activity of the Csy complex in these lysogens, we programmed the Csy complex to transcriptionally repress the *phzM* gene, which is responsible for the generation of the green pigment pyocyanin. Derepression of *phzM* expression can be quantified by measuring the accumulation of the pyocyanin pigment in an overnight culture. We found that AmrZ_{Phi3} or AmrZ_{PaBG} derepressed *phzM* to a similar extent to AcrIF4 (Fig. 4g), demonstrating anti-CRISPR activity for these hijacked CRISPR–Cas repressors.

The regulation of bacterial processes is highly variable across species, reflecting niche-specific adaptations. Here a genetic screen reveals that the KinB–AlgB two-component system regulates CRISPR–Cas in *P. aeruginosa*. Removal of KinB or inactivation of its phosphatase activity leads to the accumulation of P-AlgB, activating the CRISPR–Cas repressors AlgU, AlgR and AmrZ. This pathway also drives alginate production, which is responsible for the formation of the characteristic mucoid biofilms of cystic fibrosis *P. aeruginosa* isolates^{3,39,40}. We show that P-AlgB (via *kinB* deletion), AlgU and AlgR repress CRISPR–Cas activity during surface association and planktonic growth, and AmrZ is triggered to further repress CRISPR–Cas during surface association. Some *Pseudomonas* genetic parasites encode hijacked AmrZ homologs, which retain their ability to repress CRISPR–Cas expression and inhibit CRISPR–Cas biogenesis during lysogeny. Strikingly, we identified multiply lysogenized strains of *P. aeruginosa* with as many as four independent copies of AmrZ on mobile elements in addition to host AmrZ (Extended Data Fig. 6). The evolutionary success of AmrZ in the *Pseudomonas* mobilome and core genome suggests a 'guns for hire'⁴¹ role for this gene in the arms race between bacteria and their parasites.

We and others observed CRISPR–Cas activation^{27,28} during exponential growth, where phage infection risk is high (that is, in metabolically active, well-mixed planktonic culture²¹). Surface association lessens the infection risk, as the spatial structure limits phage dispersal and prevents a phage bloom from overtaking the entire bacterial population⁴². Although they were not measured here, spatial stratification and polysaccharide secretion in a mucoid biofilm probably also provide high levels of intrinsic phage resistance.

The observation that CRISPR–Cas expression and surface association/biofilm formation are inversely regulated is supported by our analysis of previously published PA14 transcriptomic⁴³ and proteomic⁴⁴ datasets, which show activation of CRISPR–Cas expression in exponential phase growth, and repression during stationary phase and biofilm growth at 24 and 48 h (Extended Data Fig. 7a). Cas proteins were still detected in stationary phase and biofilm growth, suggesting that the cells retained some immunity after transcriptional shutdown (Extended Data Fig. 7b). Furthermore, previous studies show that the *P. aeruginosa* genome is hypersensitive to CRISPR-induced DNA damage during surface association and biofilm formation, leading to cell death when a mismatched pro-phage sequence target is present in the chromosome^{16,17}. This suggests that CRISPR auto-immunity costs are also dependent on the growth state and physical environment of the cell.

Here we identify a CRISPR–Cas repressive pathway in *P. aeruginosa*. We speculate that the ability to control CRISPR–Cas activity during lifestyle transitions may be essential for *P. aeruginosa* to safely maintain a CRISPR–Cas system by limiting self-toxicity. In our discovery of MGE-encoded CRISPR–Cas repressors we reveal an unexpected cost to CRISPR–Cas regulation: the evolution of CRISPR–Cas repression has created an Achilles' heel that is exploited by genetic parasites.

Methods

Bacterial strains and phages. *P. aeruginosa* UCBPP-PA14 (PA14) strains and *Escherichia coli* strains (Supplementary Table 1) were grown on lysogeny broth (LB) agar or liquid at 37 °C. The media was supplemented with gentamicin (50 µg ml⁻¹ for *P. aeruginosa* and 30 µg ml⁻¹ for *E. coli*) to maintain the pHERD30T plasmid, or carbenicillin (250 µg ml⁻¹) for *P. aeruginosa* or ampicillin (100 µg ml⁻¹) for *E. coli* containing the pHERD20T plasmid. pHERD plasmids were induced with 0.1% arabinose. Phage stocks (Supplementary Table 1) were prepared as described previously¹⁸. In brief, 3 ml SM buffer was added to plate lysates of the desired purified phage and incubated at room temperature for 15 min. SM buffer containing phages was collected and 100 µl chloroform was added. This was centrifuged at 10,000g for 5 min and supernatant containing phages was transferred to a storage tube with a screw cap and incubated at 4 °C.

Transposon mutagenesis screen. The *csy::lacZ* reporter strain was subjected to transposon mutagenesis and colonies were isolated on plates containing X-gal (5-bromo-4-chloro-3-indolyl-β-D-galactopyranoside). Approximately 50,000 colonies were visually examined for increased or decreased levels of β-galactosidase and insertions were mapped by semi-random PCR. To conduct transposon mutagenesis, overnight cultures of PA14 *csy3::lacZ* and *E. coli* containing the pBTK30 Tn suicide vector were mixed in a 1:2 ratio (donor:recipient) for conjugation. Mixed cells were centrifuged at 4,000g for 10 min to pellet the cells. 100 µl resuspended conjugation pellet was then spotted on LB agar plates and incubated at 37 °C for 6 h. Conjugation spots were collected and resuspended in LB liquid media. The conjugation was then plated on LB agar plates supplemented with nalidixic acid (30 µg ml⁻¹) and gentamicin (50 µg ml⁻¹). Surviving colonies containing Tn insertions were collected into 1 ml LB liquid media. Serial dilutions of cells were prepared and plated on LB agar plates supplemented with X-gal (200 µg ml⁻¹), gentamicin (50 µg ml⁻¹) and nalidixic acid (30 µg ml⁻¹). The plates were incubated at 37 °C for 24 h to allow the colonies to change colour. Colonies displaying changed expression levels compared with the unmutagenized parental strain (PA14 *csy3::lacZ*, no pBTK30) were then isolated onto secondary LB agar plates with X-gal, gentamicin and nalidixic acid at the stated concentrations. Genomic DNA was collected from isolated single colonies by resuspending bacterial colonies in 0.02% SDS and boiling the sample for 15 min. Samples were then centrifuged at 10,000g and supernatants containing genomic DNA were collected. Transposon insertion junctions were mapped using semi-random PCR (Supplementary Table 1). PCR samples were sequenced and reads were then mapped to the *P. aeruginosa* UCBPP-PA14 genome using BLAST. Expression changes were then verified via a modified β-galactosidase assay in liquid culture.

Plaque assays. Plaque assays were performed on LB agar plates (1.5% agar) with LB top agar (0.7% agar), supplemented with MgSO₄ (10 mM final concentration), gentamicin (50 µg ml⁻¹) and arabinose (0.1%) as needed for plasmid maintenance and induction. Spot titrations were performed by mixing 150 µl *P. aeruginosa* overnight culture with 3 ml top agar, which was dispersed evenly on a LB MgSO₄ plate. 3 µl tenfold phage dilutions was then spotted on the surface and the plates were incubated overnight at 30 °C. To count the plaques, full plate assays were used, except when CRISPR targeting was so strong that discrete plaques could not be accurately measured. In this case, spot titrations are shown. For full plate assays, 10 µl of the phage dilution giving single plaques was incubated with 150 µl *P. aeruginosa* overnight culture for 10 min at 37 °C. 3 ml top agar was then added and the mixture was dispersed evenly on a LB MgSO₄ plate. Individual plaques were then counted to assess differences in the efficiency of bacterial immunity and phage efficiency of plaquing (EOP). The EOI of a bacterial mutant relative to the WT was calculated by dividing the number of p.f.u. formed on the WT by the number of p.f.u. formed on the mutant strain. An EOI > 1 means fewer plaques formed on the mutant than on the WT, so the mutant was more immune to phage infection than the WT. An EOI < 1 means more plaques formed on the mutant, so the mutant was less immune to phage infection than the WT. The EOP of a phage (Fig. 4e) was calculated by dividing the number of p.f.u. formed on the WT (CRISPR+) by the number of p.f.u. formed on ΔCRISPR. An EOP of 1 means that CRISPR does not impact phage replication; an EOP of 0 means that the phage cannot replicate in the presence of CRISPR.

β-galactosidase assay. A previously described β-galactosidase assay⁴⁵ was used to measure *lacZ* activity in transcriptional fusions. Bacterial cultures were grown overnight at 37 °C. Cultures were then diluted 1:100 into LB liquid medium supplemented with the desired antibiotic and incubated at 37 °C with shaking until the desired time point was reached. The culture density was measured with a spectrophotometer (OD₆₀₀) and 200 µl of the sample was added to 800 µl of permeabilization solution. Cells were mixed via inversion and vortexed for 1 min to permeabilize the cells. 200 µl ONPG (4 mg ml⁻¹) was added and the samples were incubated at 30 °C until the sample turned yellow. The enzymatic reaction was stopped by the addition of 300 µl 1 M Na₂CO₃. The samples were centrifuged at 13,000g for 5 min to remove debris and 200 µl supernatant was moved to a 96-well plate to read the absorbances at 420 and 550 nm. The Miller units were calculated using the Miller equation: 1 Miller unit = (1,000 × OD₄₂₀ – 1.75 × OD₅₅₀)/

($T_{\min} \times V_{\text{mi}} \times \text{OD}_{600}$), where T_{\min} indicates reaction time (min) and V_{mi} indicates reaction volume (ml).

Phage transduction of *kinB::Tn* alleles. Transposon insertions in *kinB* from a *csy3::lacZ* background were transduced into WT PA14 to test CRISPR–Cas function with the same transposon insertion. Phage phiPA3 was used to infect the donor strain (*kinB::Tn*) on plates with top agar overlays using $\sim 10^8$ p.f.u. to generate near confluent lysis. The plates were soaked in 3–4 ml of phage SM buffer and 2 ml was collected over chloroform, vortexed and pelleted to isolate the transducing phage in the supernatant. The lysates were used to infect recipient strains (WT PA14); $\sim 10^8$ p.f.u. were used to infect a culture at a multiplicity of infection of 1. After 30 min of static incubation on the bench, the cultures were gently shaken at 37 °C for 20 min and then pelleted at 5,000g. Cells were washed twice with LB and subsequently incubated at 37 °C for 1 h to allow recombination and gentamicin-resistance outgrowth. The cultures were pelleted and resuspended in 200 μ l LB and plated on LB plates containing gentamicin. The controls included uninfected cells and cells infected with phages not propagated on a gentamicin-resistant donor strain. In addition, phage lysate was directly plated under selection to confirm that there was no residual donor strain in the phage preparation. The plates were incubated overnight at 37 °C and their identity (that is, CRISPR–Cas intact) confirmed with a plaque assay using DMS3m_{acrIc3} as the target phage and PCR of the *kinB* locus.

Introduction of *csy3::lacZ* *P. aeruginosa* UCBPP-PA14 strains. The *lacZ* gene was introduced into PA14 strains of interest via allelic replacement. The recombination vector pMQ30, which contained *lacZ* flanked by homology arms matching *csy2* and *csy4*, was introduced via conjugation. PA14 strains and *E. coli* containing the vector were mixed at a ratio of 1:2 (recipient:donor). The mixture was heat shocked at 42 °C for 10 min. The mating spot was then plated on a LB agar plate and incubated overnight at 30 °C. The mating spot was then collected, resuspended in 1 ml LB liquid media and plated on VBMM plates supplemented with 50 μ g ml⁻¹ gentamicin to select for colonies with the integrated homology plasmid. The colonies were cultured overnight in LB in the absence of selection at 37 °C and were then diluted and counter-selected on no-salt LB agar plates supplemented with 15% sucrose. The surviving colonies were then grown on LB agar plates supplemented with gentamicin and X-gal to check for *lacZ* insertion via colour change; *lacZ* insertion was further verified via PCR.

RT–qPCR. Total RNA extracts were harvested using an acid–phenol chloroform extraction from liquid cultures subcultured 1:100 and grown for 8 h in LB media. RNA treated with DNase (Ambion) to remove DNA and 1 ng total RNA was used in a series of RT–qPCR reactions. The reactions were conducted in a BioRad CFX connect qPCR cycle using clear BioRad plates with the Luna Universal One-Step Reaction Mix (NEB). A standard curve for each primer set was generated using pooled RNA samples. The housekeeping gene *rpsL* was used for normalization and gene-specific primers against *cas3* and *csy3* (Supplementary Table 1) were used to quantify expression from the *cas* and *csy* operons. For RT–qPCR reactions, 1 ng total RNA was used in each reaction, performed in triplicate. Reverse transcription was conducted using Luna WarmStart RT Enzyme Mix (NEB). Standard curves were used to calculate the relative abundance of target transcripts; *cas3* and *csy3* transcript levels were then normalized to *rpsL* levels.

Generation of endogenous Csy1–sfCherry and Cas3–sfCherry reporters. Endogenous Csy1–sfCherry and Cas3–sfCherry reporters were constructed in a similar way to *csy3::lacZ*. We initially verified that Csy1 and Cas3 tagged with sfCherry at the N-terminus are functional when expressed from a plasmid. pMQ30–sfCherry–Csy1, which contains the sfCherry sequence flanked by 657 bp upstream of *csy1* and 701 bp downstream of the *csy1* start codon, was cloned in the pMQ30 plasmid between HindIII and BamHI sites using Gibson assembly. pMQ30–sfCherry–Cas3, which contains the sfCherry sequence flanked by 353 bp upstream of *cas3* and 350 bp downstream of the *cas3* start codon, was cloned in the pMQ30 plasmid between HindIII and BamHI sites using Gibson assembly. The 4 bp that overlap between the end of *cas1* and the beginning of *cas3* were duplicated in the final construct. Both pMQ30–sfCherry–Csy1 and pMQ30–sfCherry–Cas3 contain the GGAGGCGGTGGAGCC sequence (encoding GGGGA) as a linker between sfCherry and the respective tagged proteins. The Csy1–sfCherry and Cas3–sfCherry constructs were introduced into PA14 strains of interest via allelic replacement. Strains containing the appropriate insertion were verified via PCR.

sfCherry reporter profiling. *Liquid.* Cells were diluted 1:100 from an overnight culture into fresh LB (with 0.1% arabinose and 50 μ g ml⁻¹ gentamicin if required for plasmid induction and maintenance) and grown for the indicated number of hours in biological triplicate. 500 μ l of each sample was then spun down at 8,000g for 2 min and resuspended in 500 μ l M9 media. The samples were loaded onto a 96-well plate (150 μ l per well) in technical triplicate and red fluorescence (excitation, 580 nm; emission, 610 nm) and OD₆₀₀ were measured using a Biotek H4 Synergy 96-well plate reader. M9 media alone was measured to obtain a background fluorescence and absorbance reading. To calculate the relative fluorescence units (RFU) for each sample, the background fluorescence and

background OD₆₀₀ values obtained were subtracted from the sample values, and the sample fluorescence was then normalized to the sample OD₆₀₀.

Solid. Cells were diluted 1:100 from an overnight culture into fresh LB and 20 μ l was plated in individual wells in biological triplicate in a 24-well plate with each well containing solidified 1.5% LB agar (with 0.1% arabinose and 50 μ g ml⁻¹ gentamicin if required for plasmid induction and maintenance). The 24-well plate was then covered with a breathable Aeraseal and incubated at 37 °C with no shaking. At the indicated time point, the cells were harvested by flooding each well with 500 μ l M9 buffer, then spun down at 8,000g for 2 min and resuspended in 500 μ l M9 media. The samples were loaded onto a 96-well plate (150 μ l per well) in technical triplicate and red fluorescence (excitation: 580 nm; emission: 610 nm) and OD₆₀₀ were measured using a Biotek H4 Synergy 96-well plate reader. M9 media alone was measured to obtain a background fluorescence and absorbance reading. To calculate the relative fluorescence units for each sample, the background fluorescence and background OD₆₀₀ values obtained were subtracted from the sample values and the sample fluorescence was then normalized to the sample OD₆₀₀.

Generation of PA14 Δ amrZ using the endogenous I-F CRISPR–Cas system.

Complementary oligonucleotides encoding a crRNA targeting the *amrZ* gene of PA14 were annealed and ligated into the multiple cloning site of the pHERD30T vector. A fragment possessing homology arms flanking the desired mutation (500 bp upstream and 500 bp downstream) around *amrZ* was cloned into a distinct location (NheI site) of the same vector via Gibson assembly. The new plasmid containing both a crRNA and a homology region was introduced into WT PA14 via electroporation. The transformation efficiency dropped dramatically in the presence of the crRNA due to the toxicity caused by self-targeting. All surviving colonies had the desired clean deletion of the *amrZ* gene. Deletions were confirmed by PCR of the region of interest and subsequent Sanger sequencing of the amplicon. A 2,000-bp region flanking *amrZ* was PCR amplified and sequencing primers were designed to sequence the deletion junction to confirm the removal of the *amrZ* gene.

Liquid phage infection assay. Liquid phage infections were performed as described in ref. 29. In brief, an overnight culture of cells was diluted 1:100 into fresh media and infected with 10^6 p.f.u. virulent phage DMS3m_{acrIc4} in biological triplicate in a 96-well Costar plate. Cells were incubated at 37 °C with constant rotation and the OD₆₀₀ was measured every 5 min in a Biotek H4 Synergy plate reader. Phages were harvested from each well and quantified by plaque assay after 24 h. In these experiments, all strains used in the assays carried two spacers against the DMS3m_{acrIc4} phage to prevent phage escape: one endogenous spacer (CRISPR2_sp1) and one provided on a pHERD30T plasmid.

AmrZ homolog discovery and characterization. BLASTp was used to search the non-redundant protein database for AmrZ homologs (accession: [ABJ12639.1](#)) in December 2018 using BLAST v.2.8.1 (ref. 46). This homolog list (e value > 0.001, where e represents the expect value) was then examined for homologs found on phage or plasmid genomes. Representative homologs were aligned using Clustal Omega v.1.2.2 (ref. 47) and the alignment visualized in Jalview v.2.10.02 (ref. 48). Key conserved residues were mapped onto the structure in Pymol v.2.0.7 (PDB ID: 3QQQ). Select homologs were synthesized (TWIST Biosciences) and cloned into the SacI/PstI site of the arabinose-inducible plasmid pHERD30T using Gibson assembly. Vectors were electroporated into *P. aeruginosa* strains for functional testing, where they were induced with 0.1% arabinose and maintained with 50 μ g ml⁻¹ gentamicin.

Construction of recombinant DMS3m AmrZ phages. Phages were generated as previously described²⁹. Briefly, Gibson assembly was used to generate a recombination plasmid on pHERD30T with *amrZ*_{phi3} or *amrZ*_{pubG} flanked by homology arms up and downstream of the DMS3m Acr locus. This plasmid was transformed into PA14 Δ CRISPR and infected with phage DMS3m_{acr-gent} (a phage that is sick as a result of the insertion of a large gentamicin-resistance cassette into its anti-CRISPR locus). Healthy plaques resulting from the recombination were screened using PCR for incorporation of *amrZ*_{phi3} or *amrZ*_{pubG} into the anti-CRISPR locus.

Construction of PA14 lysogens. Lysogens were obtained by first spotting phage onto a bacterial lawn, then streaking out surviving colonies from phage spots. These colonies were screened for phage resistance using a cross-streak method and lysogeny was verified by prophage induction.

Pyocyanin repression assay. The pyocyanin repression assay was performed as previously described²⁵. Lysogens were transformed with a plasmid encoding a Type I-F crRNA targeting the promoter region of the gene *phzM*, which is required for the synthesis of the green pigment pyocyanin. As a control, each lysogen was also transformed with the empty vector. These strains were grown overnight (~16 h) in 5 ml LB media supplemented with 50 μ g ml⁻¹ gentamicin and 0.1% arabinose, to induce crRNA expression. Pyocyanin was extracted with an equal volume of

chloroform and then mixed with a half volume of 0.2 M HCl, which produces a pink colour proportional to the amount of pyocyanin and can be quantified by measuring absorbance at 520 nm. The absorbance value of each crRNA-expressing lysogen was expressed as a percentage of the pyocyanin level measured in the EV control lysogen. Samples were measured in technical triplicate.

Statistical testing. This study used a two-tailed unpaired Student's *t* test for statistical testing. In all cases, the sample size was $n = 3$, the degrees of freedom $n - 1$ and the confidence interval 95%. In all plots, bar or data point height is equivalent to the mean and error bars are shown as ± 1 s.d.

Reporting Summary. Further information on research design is available in the Nature Research Reporting Summary linked to this article.

Data availability

Source data and statistics used to generate figures are provided with the paper. Additional data supporting the findings of this paper are available from the corresponding author on request.

Received: 27 June 2019; Accepted: 12 February 2020;

Published online: 23 March 2020

References

- Barrangou, R. et al. CRISPR provides acquired resistance against viruses in prokaryotes. *Science* **315**, 1709–1712 (2007).
- Brouns, S. J. J. et al. Small CRISPR RNAs guide antiviral defense in prokaryotes. *Science* **321**, 960–964 (2008).
- Damron, F. H., Qiu, D. & Yu, H. D. The *Pseudomonas aeruginosa* sensor kinase KinB negatively controls alginate production through AlgW-dependent MucA proteolysis. *J. Bacteriol.* **191**, 2285–2295 (2009).
- Damron, F. H. et al. Analysis of the *Pseudomonas aeruginosa* regulon controlled by the sensor kinase KinB and sigma factor RpoN. *J. Bacteriol.* **194**, 1317–1330 (2012).
- Wozniak, D. J. & Ohman, D. E. Transcriptional analysis of the *Pseudomonas aeruginosa* genes *algR*, *algB*, and *algD* reveals a hierarchy of alginate gene expression which is modulated by *algT*. *J. Bacteriol.* **176**, 6007–6014 (1994).
- Baynham, P. J. & Wozniak, D. J. Identification and characterization of AlgZ, an AlgT-dependent DNA-binding protein required for *Pseudomonas aeruginosa* *algD* transcription. *Mol. Microbiol.* **22**, 97–108 (1996).
- Hochstrasser, M. L. et al. CasA mediates Cas3-catalyzed target degradation during CRISPR RNA-guided interference. *Proc. Natl Acad. Sci. USA* **111**, 6618–6623 (2014).
- Westra, E. R. et al. CRISPR immunity relies on the consecutive binding and degradation of negatively supercoiled invader DNA by Cascade and Cas3. *Mol. Cell* **46**, 595–605 (2012).
- Levy, A. et al. CRISPR adaptation biases explain preference for acquisition of foreign DNA. *Nature* **520**, 505–510 (2015).
- Haurwitz, R. E., Jinek, M., Wiedenheft, B., Zhou, K. & Doudna, J. A. Sequence- and structure-specific RNA processing by a CRISPR endonuclease. *Science* **329**, 1355–1358 (2010).
- Wiedenheft, B. et al. Structural basis for DNase activity of a conserved protein implicated in CRISPR-mediated genome defense. *Structure* **17**, 904–912 (2009).
- Wiedenheft, B. et al. RNA-guided complex from a bacterial immune system enhances target recognition through seed sequence interactions. *Proc. Natl Acad. Sci. USA* **108**, 10092–10097 (2011).
- Rollins, M. F., Schuman, J. T., Paulus, K., Bukhari, H. S. T. & Wiedenheft, B. Mechanism of foreign DNA recognition by a CRISPR RNA-guided surveillance complex from *Pseudomonas aeruginosa*. *Nucleic Acids Res.* **43**, 2216–2222 (2015).
- Rollins, M. F. et al. Cas1 and the Csy complex are opposing regulators of Cas2/3 nuclease activity. *Proc. Natl Acad. Sci. USA* **114**, E5113–E5121 (2017).
- Chowdhury, S. et al. Structure reveals mechanisms of viral suppressors that intercept a CRISPR RNA-guided surveillance complex. *Cell* **169**, 47–57 (2017).
- Zegans, M. E. et al. Interaction between bacteriophage DMS3 and host CRISPR region inhibits group behaviors of *Pseudomonas aeruginosa*. *J. Bacteriol.* **191**, 210–219 (2009).
- Cady, K. C. & O'Toole, G. A. Non-identity-mediated CRISPR-bacteriophage interaction mediated via the Csy and Cas3 proteins. *J. Bacteriol.* **193**, 3433–3445 (2011).
- Cady, K. C., Bondy-Denomy, J., Heussler, G. E., Davidson, A. R. & O'Toole, G. A. The CRISPR/Cas adaptive immune system of *Pseudomonas aeruginosa* mediates resistance to naturally occurring and engineered phages. *J. Bacteriol.* **194**, 5728–5738 (2012).
- Vorontsova, D. et al. Foreign DNA acquisition by the I-F CRISPR–Cas system requires all components of the interference machinery. *Nucleic Acids Res.* **43**, 10848–10860 (2015).
- van Belkum, A. et al. Phylogenetic distribution of CRISPR–Cas systems in antibiotic-resistant *Pseudomonas aeruginosa*. *mBio* **6**, e01796–15 (2015).
- Westra, E. R. et al. Parasite exposure drives selective evolution of constitutive versus inducible defense. *Curr. Biol.* **25**, 1043–1049 (2015).
- van Houte, S. et al. The diversity-generating benefits of a prokaryotic adaptive immune system. *Nature* **532**, 385–388 (2016).
- Bondy-Denomy, J., Pawluk, A., Maxwell, K. L. & Davidson, A. R. Bacteriophage genes that inactivate the CRISPR/Cas bacterial immune system. *Nature* **493**, 429–432 (2013).
- Pawluk, A., Bondy-Denomy, J., Cheung, V. H. W., Maxwell, K. L. & Davidson, A. R. A new group of phage anti-CRISPR genes inhibits the type I-E CRISPR–Cas system of *Pseudomonas aeruginosa*. *mBio* **5**, e00896–14 (2014).
- Bondy-Denomy, J. et al. Multiple mechanisms for CRISPR–Cas inhibition by anti-CRISPR proteins. *Nature* **526**, 136–139 (2015).
- Pawluk, A. et al. Inactivation of CRISPR–Cas systems by anti-CRISPR proteins in diverse bacterial species. *Nat. Microbiol.* **1**, 16085 (2016).
- Høyland-Kroghsbo, N. M. et al. Quorum sensing controls the *Pseudomonas aeruginosa* CRISPR–Cas adaptive immune system. *Proc. Natl Acad. Sci. USA* **114**, 131–135 (2016).
- Patterson, A. G. et al. Quorum sensing controls adaptive immunity through the regulation of multiple CRISPR–Cas systems. *Mol. Cell* **64**, 1102–1108 (2016).
- Borges, A. L. et al. Bacteriophage cooperation suppresses CRISPR–Cas3 and Cas9 immunity. *Cell* **174**, 917–925 (2018).
- Chand, N. S. et al. The sensor kinase KinB regulates virulence in acute *Pseudomonas aeruginosa* infection. *J. Bacteriol.* **193**, 2989–2999 (2011).
- Chand, N. S., Clatworthy, A. E. & Hung, D. T. The two-component sensor KinB acts as a phosphatase to regulate *Pseudomonas aeruginosa* virulence. *J. Bacteriol.* **194**, 6537–6547 (2012).
- Cezairliyan, B. O. & Sauer, R. T. Control of *Pseudomonas aeruginosa* AlgW protease cleavage of MucA by peptide signals and MucB. *Mol. Microbiol.* **72**, 368–379 (2009).
- Schurr, M. J., Yu, H., Martinez-Salazar, J. M., Boucher, J. C. & Deretic, V. Control of AlgU, a member of the sigma E-like family of stress sigma factors, by the negative regulators MucA and MucB and *Pseudomonas aeruginosa* conversion to mucoidy in cystic fibrosis. *J. Bacteriol.* **178**, 4997–5004 (1996).
- Tart, A. H., Blanks, M. J. & Wozniak, D. J. The AlgT-dependent transcriptional regulator AmrZ (AlgZ) inhibits flagellum biosynthesis in mucoid, nonmotile *Pseudomonas aeruginosa* cystic fibrosis isolates. *J. Bacteriol.* **188**, 6483–6489 (2006).
- Schulz, S. et al. Elucidation of sigma factor-associated networks in *Pseudomonas aeruginosa* reveals a modular architecture with limited and function-specific crosstalk. *PLoS Pathog.* **11**, e1004744 (2015).
- Wozniak, D. J. et al. Alginate is not a significant component of the extracellular polysaccharide matrix of PA14 and PAO1 *Pseudomonas aeruginosa* biofilms. *Proc. Natl Acad. Sci. USA* **100**, 7907–7912 (2003).
- Pratama, A. A. & van Elsland, J. D. A novel inducible prophage from the mycosphere inhabitant *Paraburkholderia terrae* BS437. *Sci. Rep.* **7**, 9156 (2017).
- Pryor, E. E. et al. The transcription factor AmrZ utilizes multiple DNA binding modes to recognize activator and repressor sequences of *Pseudomonas aeruginosa* virulence genes. *PLoS Pathog.* **8**, e1002648 (2012).
- Martin, D. W. et al. Mechanism of conversion to mucoidy in *Pseudomonas aeruginosa* infecting cystic fibrosis patients. *Proc. Natl Acad. Sci. USA* **90**, 8377–8381 (1993).
- Jones, A. K. et al. Activation of the *Pseudomonas aeruginosa* AlgU regulon through *mucA* mutation inhibits cyclic AMP/Vfr signaling. *J. Bacteriol.* **192**, 5709–5717 (2010).
- Koonin, E. V. & Makarova, K. S. Mobile genetic elements and evolution of CRISPR–Cas systems: all the way there and back. *Genome Biol. Evol.* **9**, 2812–2825 (2017).
- Heilmann, S., Sneppen, K. & Krishna, S. Sustainability of virulence in a phage-bacterial ecosystem. *J. Virol.* **84**, 3016–3022 (2010).
- Dötsch, A. et al. The *Pseudomonas aeruginosa* transcriptional landscape is shaped by environmental heterogeneity and genetic variation. *mBio* **6**, e00749–15 (2015).
- Erdmann, J., Preusse, M., Khaledi, A., Pich, A. & Häussler, S. Environment-driven changes of mRNA and protein levels in *Pseudomonas aeruginosa*. *Environ. Microbiol.* **20**, 3952–3963 (2018).
- Smale, S. T. β -galactosidase assay. *Cold Spring Harb. Protoc.* <https://doi.org/10.1101/pdb.prot5423> (2010).
- Altschul, S. F., Gish, W., Miller, W., Myers, E. W. & Lipman, D. J. Basic local alignment search tool. *J. Mol. Biol.* **215**, 403–410 (1990).
- Sievers, F. et al. Fast, scalable generation of high-quality protein multiple sequence alignments using Clustal Omega. *Mol. Syst. Biol.* **7**, 539 (2011).
- Waterhouse, A. M., Procter, J. B., Martin, D. M. A., Clamp, M. & Barton, G. Jalview Version 2—a multiple sequence alignment editor and analysis workbench. *Bioinformatics* **25**, 1189–1191 (2009).

49. Arndt, D. et al. PHASTER: a better, faster version of the PHAST phage search tool. *Nucleic Acids Res.* **44**, W16–W21 (2016).

Acknowledgements

We thank D. Hung's lab for providing $\Delta kinB$, $\Delta algB$, $\Delta algR$ and $\Delta algU$ mutants and G. O'Toole's lab for providing the *csy3::lacZ* PA14 strain. We thank K. Trotta (S. Chou's lab, UCSF) for advice in the development of fluorescent assays and A. Santiago-Frangos (B. Wiedenheft's lab, MSU) for advice and consultation. J.B.-D.'s lab was supported by the UCSF Program for Breakthrough in Biomedical Research (funded in part by the Sandler Foundation), the Innovative Genomics Institute, a National Institutes of Health Office of the Director Early Independence Award (no. DP5-OD021344) and grant no. R01GM127489.

Author contributions

J.B.-D., A.L.B. and B.C. formulated the study design and plans. A.L.B. performed CRISPR–Cas activity and expression profiling and conducted bioinformatics analyses. B.C. conducted the genetic screen and constructed and characterized bacterial mutants.

S.G. constructed sfCherry reporter strains. T.S. conducted CRISPRi assays. V.E. assisted in establishing reporter assays. J.B.-D. and A.L.B. wrote the manuscript.

Competing interests

J.B.-D. is a scientific advisory board member of SNIPR Biome and Excision Biotherapeutics and a scientific advisory board member and cofounder of Acrigen Biosciences.

Additional information

Supplementary information is available for this paper at <https://doi.org/10.1038/s41564-020-0691-3>.

Extended data is available for this paper at <https://doi.org/10.1038/s41564-020-0691-3>.

Correspondence and requests for materials should be addressed to J.B.-D.

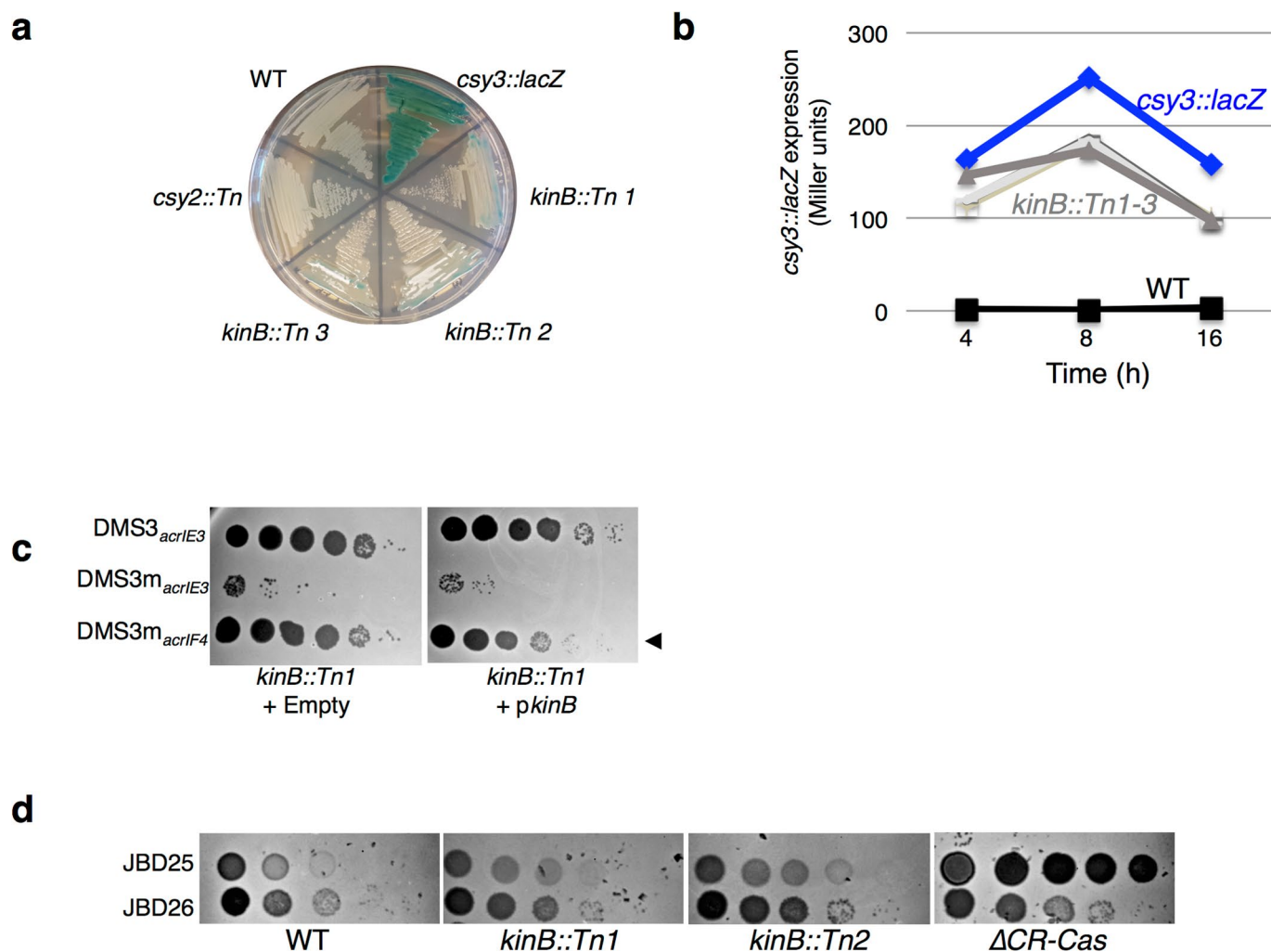
Reprints and permissions information is available at www.nature.com/reprints.

Publisher's note Springer Nature remains neutral with regard to jurisdictional claims in published maps and institutional affiliations.

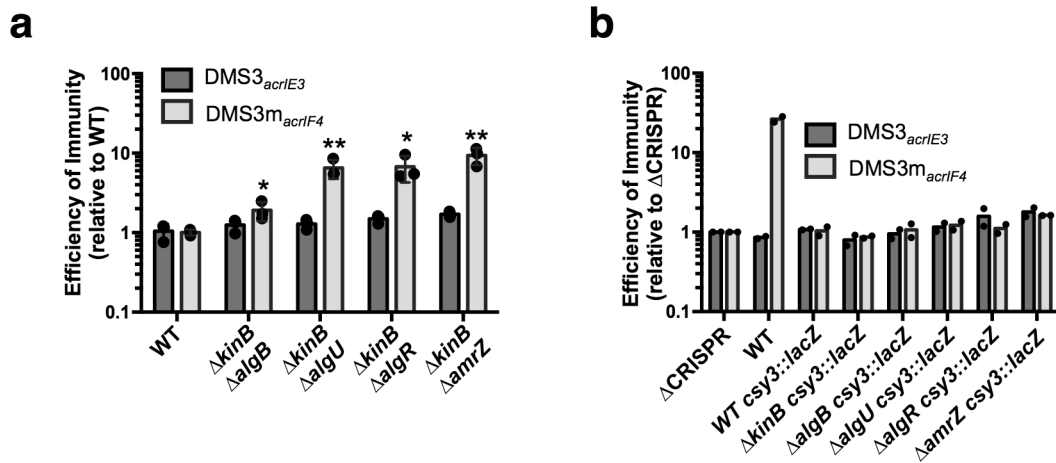
© The Author(s), under exclusive licence to Springer Nature Limited 2020

Gene with insertion	Transposon Location	β -gal activity (% unmutagenized)
pchH	797705	127%
pchH	798159	131%
S-type pyocin	1196879	145%
putative membrane protein	1400718	118%
minD	1915545	N/D (growth defect)
deaD	2373899	N/D (growth defect)
putative Zn-dependent oxidoreductase	2820446	115% (growth defect)
gnyL	3434168	87%
bacA	3490006	75%
Intergenic; zipA and smc + lasR	3979746	N/D (growth defect)
	4085810	135%
oxidoreductase FMN binding	4188602	N/D (growth defect)
pyoS3A	4404303	145%
tolA	4595505	158%
purM	4618060	134%
Intergenic; fstA and fstZ	5104077	111% (growth defect)
cytochrome c1 precursor	5126449	94%
putative plasmid stabilization protein	5347104	N/D (growth defect)
paraquat inducible protein	5532785	108%
glycosyl transferase	5889967	81%
gltB	5943637	108%
yhiH/yhil	6162134	108%
crc	6275250	91%
kinB (3)	6447811	53%
kinB (2)	6447945	50%
kinB (1)	6448519	59%
kinB (5)	6449345	98%
kinB (4)	6449373	54%
polA	6457284	N/D (growth defect)
gidB	6530337	88%

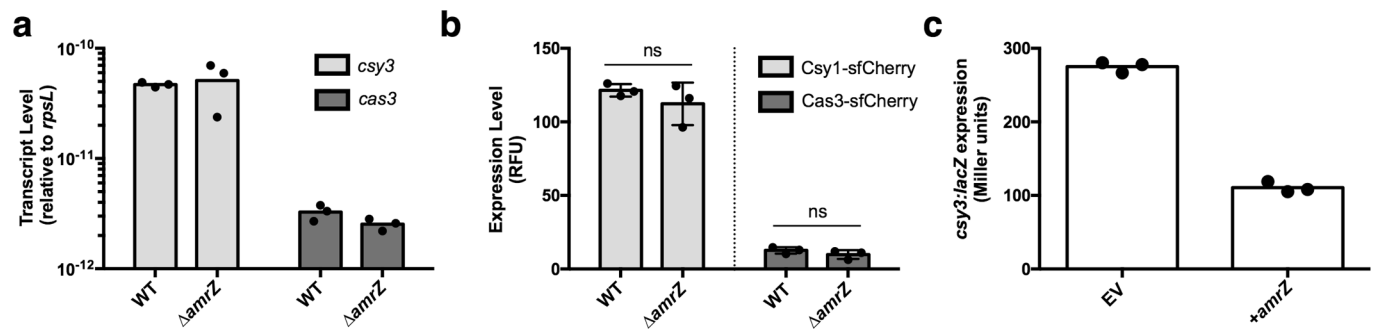
Extended Data Fig. 1 | Mapped insertions from transposon mutagenesis screen. All independent transposon insertions identified and mapped by visual screening with increased or decreased *csy3::lacZ* β -galactosidase activity. β -galactosidase activity is expressed as a percentage of the unmutagenized parent strain, and measurements were taken at a single timepoint after 8 h of growth in liquid culture. The insertion location in the PA14 genome is shown, along with the measured level of β -galactosidase enzyme at the 8 hour timepoint. These measurements were not determined (N/D) for strains with a growth defect.



Extended Data Fig. 2 | Characterization of $kinB::Tn$ mutants. **a.** A streak plate on X-gal plates, showing strains involved in this study and isolated transposon (Tn) insertions. $csy3::lacZ$ is a derivative of WT PA14, and is the unmutagenized parent of $kinB::Tn$ 1-3. **b.** β -galactosidase measurements of strains grown in liquid culture for the indicated time. Measurements for the unmutagenized ($csy3::lacZ$) parent strain and three isolated $kinB$ transposon mutants ($kinB::Tn1-3$) are shown, as well as a control PA14 culture with no $lacZ$ insertion. **c.** Phage titration on lawns of the $kinB::Tn1$ mutant transformed with empty vector or $kinB$. **d.** Spot titration of phages JBD26 (CR2_sp17, sp20-targeted, possessing $acrIF4$), JBD25 (CR1_sp1 targeted) on $kinB::Tn$ mutants and ΔCR -Cas. These experiments have been replicated at least 2 times with consistent results.



Extended Data Fig. 3 | Double knockouts of pathway members. a, b. Efficiency of immunity measurements for indicated mutants relative to WT. a. Double knockouts show $\Delta kinB$ combined with *algB*, *algU*, *algR*, or *amrZ*. EOI measurements are shown as the mean of 3 biological replicates, \pm S.D. Mutants show increased EOI against DMS3m_{acrF4} relative to WT ($\Delta kinB \Delta algB$, $P = 3.8 \times 10^{-2}$, $\Delta kinB \Delta algU$, $P = 5.9 \times 10^{-3}$, $\Delta kinB \Delta algR$, $P = 1.5 \times 10^{-2}$, $\Delta kinB \Delta amrZ$, $P = 3.2 \times 10^{-3}$). Two-tailed unpaired Student's T-test was used to calculate P value, * $p < 0.05$, ** $p < 0.01$. b. Indicated knockouts were combined with *csy3::lacZ*, EOI shown as the mean of two biological replicates. These experiments have been replicated at least 2 times with consistent results.



Extended Data Fig. 4 | *AmrZ* activity in liquid growth. **a.** qRT-PCR measurements of transcript levels of *csy3* (light grey) and *cas3* (dark grey) normalized to the housekeeping gene *rpsL* after 8 h of growth in liquid culture. Measurements are represented as the mean of 3 technical replicates. **b.** Measurement of the fluorescence levels of Csy1-sfCherry (light grey) or Cas3-sfCherry (dark grey) reporter strains after 10 h of growth in liquid culture. Fluorescence measurements are represented as the mean of 3 biological replicates \pm SD. Cas3-sfCherry ($P=0.26$) and Csy1-sfCherry levels ($P=0.35$) in $\Delta amrZ$ did not differ significantly from WT. Two-tailed unpaired Student's T-test was used to calculate P value, ns = not significant. **c.** *csy3::lacZ* β -galactosidase activity from PA14 WT *csy3::lacZ* transformed with either empty vector (EV) or a plasmid overexpressing *AmrZ* (+*AmrZ*). β -galactosidase reporter activity was measured after 8 h in liquid growth and is represented as the mean of 3 technical replicates. Experiment was replicated two times with consistent results.

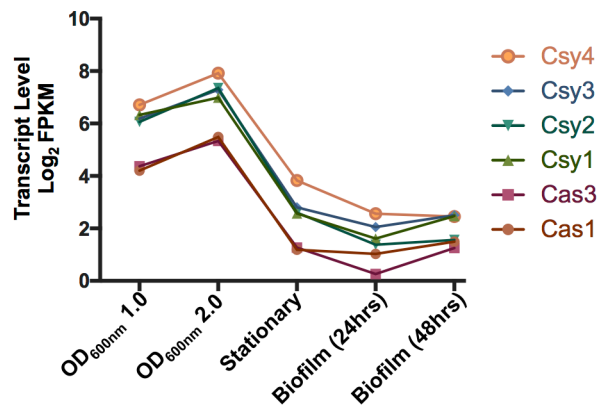
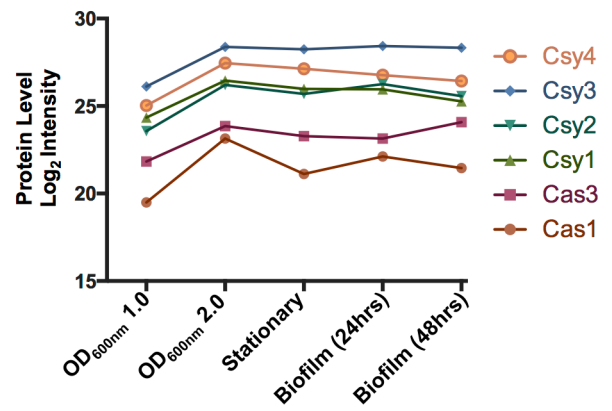
Name	Accession	MGE type
PA14 AmrZ	ABJ12639.1	
<i>Pseudomonas</i> phage Noxifer	ARV77275.1	Lytic Myovirus
<i>Pseudomonas</i> phage phi3	YP_009276432.1	Integrated prophage
<i>Pseudomonas</i> phage PaBG	YP_008433620.1	Lytic Myovirus
<i>Pseudomonas</i> phage SM1	ALT58107.1	Siphoviridae (temperate)
<i>Pseudomonas</i> phage F10	YP_001293379.1	Siphoviridae (temperate)
<i>Pseudomonas</i> phage JBD68	ARM70500.1	Siphoviridae (temperate)
<i>Pseudomonas</i> sp. VLB120 plasmid pSTY	AGZ38169.1	Plasmid
<i>Pseudomonas putida</i> plasmid pKF715B	BAW27310.1	Plasmid
<i>Pseudomonas veronii</i> plasmid PVE plasmid	SBW85251.1	Plasmid
<i>Pseudomonas koreensis</i> plasmid p3	AVX93364.1	Plasmid
<i>Pseudomonas</i> sp. Leaf58 plasmid pBASL58	AYG48213.1	Plasmid
<i>Pseudomonas</i> sp. XWY-1 plasmid	AUZ62175.1	Plasmid
<i>Pseudomonas putida</i> KF715C pA870	BAW26592.1	Plasmid
<i>Pseudomonas putida</i> S12 plasmid pTTS12	AJA17154.1	Plasmid
<i>Pseudomonas putida</i> p12969-DIM	ALZ46341.1	Plasmid

Extended Data Fig. 5 | Mobile AmrZ homologs. AmrZ homologs listed by the genome that encodes them, the accession number, and the mobile genetic element type.

Pseudomonas aeruginosa strain FDAARGOS_570, CP033835.1	Accession	Genomic coordinates
AmrZ-1	AYZ87048.1	6274191 to 6274418, JBD68-like prophage
AmrZ-2	AYZ83165.1	1992281 to 1992508, JBD68-like prophage
AmrZ-3	AYZ81620.1	292461 to 292688, JBD68-like prophage
AmrZ-4	AYZ82758.1	1562237 to 1562392, phi3-like prophage
AmrZ-5	AYZ86193.1	5356309 to 5356461, core genome (endogenous AmrZ)

Pseudomonas aeruginosa strain PA11803, CP015003.1	Accession	Genomic coordinates
AmrZ-1	AOX38089.1	1366154 to 1366381, unknown prophage type
AmrZ-2	AOX38026.1	1323851 to 1324078, JBD68-like prophage
AmrZ-3	AOX37649.1	937493 to 937720, JBD68-like prophage
AmrZ-4	AOX37592.1	896299 to 896526, JBD68-like prophage
AmrZ-5	AOX38565.1	1866517 to 1866654, core genome (endogenous AmrZ)

Extended Data Fig. 6 | AmrZ copy number analysis of two *Pseudomonas aeruginosa* strains. AmrZ copy number analysis of two different strains of *Pseudomonas aeruginosa*. AmrZ homologs listed by accession number and their genomic coordinates. Phaster⁴⁹ was used to identify the prophages encoding mobile AmrZ copies.

a**b**

Extended Data Fig. 7 | *Cas* and *Csy* RNA and protein levels across growth conditions. **a.** Log₂ of Fragments Per Kilobase of transcript per Million mapped reads (FPKM) shown for each I-F *cas* gene in PA14 in the indicated growth condition⁴³. **b.** Log₂ of protein levels for each of the I-F *Cas* proteins in PA14 in the indicated growth condition⁴⁴.

Reporting Summary

Nature Research wishes to improve the reproducibility of the work that we publish. This form provides structure for consistency and transparency in reporting. For further information on Nature Research policies, see [Authors & Referees](#) and the [Editorial Policy Checklist](#).

Statistics

For all statistical analyses, confirm that the following items are present in the figure legend, table legend, main text, or Methods section.

n/a Confirmed

- | | | |
|-------------------------------------|-------------------------------------|--|
| <input type="checkbox"/> | <input checked="" type="checkbox"/> | The exact sample size (n) for each experimental group/condition, given as a discrete number and unit of measurement |
| <input type="checkbox"/> | <input checked="" type="checkbox"/> | A statement on whether measurements were taken from distinct samples or whether the same sample was measured repeatedly |
| <input type="checkbox"/> | <input checked="" type="checkbox"/> | The statistical test(s) used AND whether they are one- or two-sided
<i>Only common tests should be described solely by name; describe more complex techniques in the Methods section.</i> |
| <input checked="" type="checkbox"/> | <input type="checkbox"/> | A description of all covariates tested |
| <input checked="" type="checkbox"/> | <input type="checkbox"/> | A description of any assumptions or corrections, such as tests of normality and adjustment for multiple comparisons |
| <input type="checkbox"/> | <input checked="" type="checkbox"/> | A full description of the statistical parameters including central tendency (e.g. means) or other basic estimates (e.g. regression coefficient) AND variation (e.g. standard deviation) or associated estimates of uncertainty (e.g. confidence intervals) |
| <input type="checkbox"/> | <input checked="" type="checkbox"/> | For null hypothesis testing, the test statistic (e.g. F , t , r) with confidence intervals, effect sizes, degrees of freedom and P value noted
<i>Give P values as exact values whenever suitable.</i> |
| <input checked="" type="checkbox"/> | <input type="checkbox"/> | For Bayesian analysis, information on the choice of priors and Markov chain Monte Carlo settings |
| <input checked="" type="checkbox"/> | <input type="checkbox"/> | For hierarchical and complex designs, identification of the appropriate level for tests and full reporting of outcomes |
| <input checked="" type="checkbox"/> | <input type="checkbox"/> | Estimates of effect sizes (e.g. Cohen's d , Pearson's r), indicating how they were calculated |

Our web collection on [statistics for biologists](#) contains articles on many of the points above.

Software and code

Policy information about [availability of computer code](#)

Data collection

Pictures of plaque assays and gels were taken using Image Lab (TM) Version 6.0.1 (C) 2017, Bio-Rad Laboratories, Inc. Growth curve assays were collected using BioTek Synergy H1 software Gen5 3.05.11.

Data analysis

Data were analyzed in Microsoft Excel Version 14.6.7 and plotted using GraphPad Prism 6.0 software. Clustal Omega was used to generate a multiple sequence alignment for AmrZ homologs through the EMBL-EBI webform on April 25, 2019. Sequence alignments were visualized using Jalview 2, version 2.10.2. PBD structures were visualized using PyMol, version 2.0.7.

For manuscripts utilizing custom algorithms or software that are central to the research but not yet described in published literature, software must be made available to editors/reviewers. We strongly encourage code deposition in a community repository (e.g. GitHub). See the Nature Research [guidelines for submitting code & software](#) for further information.

Data

Policy information about [availability of data](#)

All manuscripts must include a [data availability statement](#). This statement should provide the following information, where applicable:

- Accession codes, unique identifiers, or web links for publicly available datasets
- A list of figures that have associated raw data
- A description of any restrictions on data availability

Source data and statistics used to generate Figures 1-4 and Extended Data Figures 2-4 are provided with the paper. Additional data supporting the findings of this paper will be made available from the corresponding author by request.

Field-specific reporting

Please select the one below that is the best fit for your research. If you are not sure, read the appropriate sections before making your selection.

Life sciences Behavioural & social sciences Ecological, evolutionary & environmental sciences

For a reference copy of the document with all sections, see [nature.com/documents/nr-reporting-summary-flat.pdf](https://www.nature.com/documents/nr-reporting-summary-flat.pdf)

Life sciences study design

All studies must disclose on these points even when the disclosure is negative.

Sample size	No sample size calculation was performed to determine sample size. The majority of experiments use a sample size of three, as is standard in the field. This study uses isogenic, clonal bacterial strains that show a high degree of reproducibility.
Data exclusions	No data were excluded.
Replication	Phage quantification (efficiency of plaquing, efficiency of immunity, total PFU counts, etc) and growth curves were all performed at least twice, showing replication each time. Here we show representative examples. Pictures of plaque assays shown are representative examples of phenotypes observed throughout the sample(s), with consistent results seen between replicates. lacZ activity profiling of csy3:lacZ and sfCherry measurements were replicated for each mutant two times or more, with consistent results seen. Pyocyanin repression was visually assessed in three independent replicates with consistent results seen. Pyocyanin levels were quantified for representative samples.
Randomization	Samples were organized into experimental groups depending on genotype, including genes and crRNAs encoded by the bacterial strain. Randomization was not performed in this study.
Blinding	Blinding was not performed in this study, all results are quantitative. No group allocation occurred.

Reporting for specific materials, systems and methods

We require information from authors about some types of materials, experimental systems and methods used in many studies. Here, indicate whether each material, system or method listed is relevant to your study. If you are not sure if a list item applies to your research, read the appropriate section before selecting a response.

Materials & experimental systems

n/a	Involved in the study
<input checked="" type="checkbox"/>	<input type="checkbox"/> Antibodies
<input checked="" type="checkbox"/>	<input type="checkbox"/> Eukaryotic cell lines
<input checked="" type="checkbox"/>	<input type="checkbox"/> Palaeontology
<input type="checkbox"/>	<input checked="" type="checkbox"/> Animals and other organisms
<input checked="" type="checkbox"/>	<input type="checkbox"/> Human research participants
<input checked="" type="checkbox"/>	<input type="checkbox"/> Clinical data

Methods

n/a	Involved in the study
<input checked="" type="checkbox"/>	<input type="checkbox"/> ChIP-seq
<input checked="" type="checkbox"/>	<input type="checkbox"/> Flow cytometry
<input checked="" type="checkbox"/>	<input type="checkbox"/> MRI-based neuroimaging

Animals and other organisms

Policy information about [studies involving animals](#); [ARRIVE guidelines](#) recommended for reporting animal research

Laboratory animals	This study did not involve laboratory animals
Wild animals	This study did not involve wild animals
Field-collected samples	This study did not involve field collected samples
Ethics oversight	No ethical approval was required as this study uses only phages and bacteria which do not require ethical oversight in their study.

Note that full information on the approval of the study protocol must also be provided in the manuscript.